Materials Horizons

ROYAL SOCIETY OF CHEMISTRY

COMMUNICATION

View Article Online
View Journal | View Issue

Check for updates

Cite this: *Mater. Horiz.*, 2022, 9, 368

Received 30th July 2021,
Accepted 6th September 2021

DOI: 10.1039/d1mh01207j

rsc.li/materials-horizons

Published on 06 September 2021. Downloaded on 5/21/2025 1:41:29 AM.

Multi-photoresponsive triphenylethylene derivatives with photochromism, photodeformation and room temperature phosphorescence†

Yunhao Fan,[a] Mengmeng Han,[a] Arui Huang,[a] Qiuyan Liao,[a] Jin Tu,[a] Xiuxing Liu,[a] Bohan Huang,[a] Qianqian Li*[a] and Zhen Li *[ab]

A series of triphenylethylene derivatives exhibited multi-photoresponsive properties, including photochromism, photodeformation and room temperature phosphorescence (RTP), which are strongly related to molecular conformations and packing in the aggregated states. Accordingly, these properties can be subtly adjusted by substituents to the center double bond and/or peripheral phenyl moieties. The introduction of bromine atom was beneficial to photochromism and photodeformation properties as a result of the additional C–H···Br interactions and electron-withdrawing property. Also, it can promote the RTP effect *via* heavy atom effect, resulting in persistent afterglow lasting up to 150 min as detected by chemiluminescent imaging system.

New concepts

Various photoresponsive properties, including photochromism, photodeformation and room temperature phosphorescence (RTP), have been attracting increasing interest and exhibit potential applications in photoswitches, photoactuators, chemo-/biosensors, data encryption and 3D printing. However, they are seldom combined in one compound, partially because of the varied responsive mechanisms under UV irradiation, which are dependent on the dynamic molecular aggregates formed under different conditions. In this text, multi-photoresponsive properties were realized in triphenylethylene derivatives with adjustable molecular aggregates by the introduction of different substituents, providing a platform to investigate inherent mechanisms and related applications. The incorporation of electron-withdrawing moieties can improve the photochromism and photodeformation performance by a promoted photoinduced cyclization process, and the RTP effect was produced *via* heavy atom effect and optimized aggregation structures in the crystalline state. These multiple photoresponsive properties can integrate the applications from photochromism, photodeformation and RTP into a single component, which can promote the development of smart materials actuated by light irradiation.

Introduction

Photoresponsive properties have a tremendous impact on advanced materials, as they can endow static materials with dynamic properties, including changes of color, shape and emission. These changeable properties are mainly due to the varied molecular structures and aggregated forms present under different conditions, and are determined by possible photoinduced molecular motions and chemical reactions in most cases. For photochromic properties, isomerization induced by irradiation with at least two states is required.[1–10] Furthermore, the two isomers should exhibit different colors caused by discrepant conjugated subjects.[11–16] This reversible photoisomerization as photochemical driving force can result in a photodeformable property in some cases, demonstrating the double switch of color and shape under light stimulus.[17–23] It can be further optimized by the aid of a polymer matrix.[24–31] However, the photoluminescence property is seldom connected with these photoswitchable properties, because of the possible energy loss in photochromic and photodeformable processes. Especially, room temperature phosphorescence (RTP), which is sensitive to molecular motions in excited states, is hard to achieve in the dynamic state by UV irradiation.[32–36] Moreover, the efficient intersystem crossing (ISC) process and stable triplet excited states as the required elements for RTP are difficult to realize in organic materials, partially due to the weak spin–orbit coupling (SOC) between singlet and triplet excited states.[37–42]

Thus, achieving a combination of various photoresponsive properties is a complex and challenging task, because of the different requirements and possible contradictions in the

[a] *Hubei Key Lab on Organic and Polymeric Opto-Electronic Materials, Sauvage Center for Molecular Sciences, Department of Chemistry, Wuhan University, Wuhan 430072, China. E-mail: liqianqian@whu.edu.cn, lizhen@whu.edu.cn*
[b] *Institute of Molecular Aggregation Science, Tianjin University, Tianjin 300072, China*

† Electronic supplementary information (ESI) available. CCDC 2094578, 2094580, 2094581, 2094582, 2094587 and 2094588 contain the supplementary crystallographic data of TPM, TPMBr, TPMBr2, TPF, TPFBr and TPFBr2, respectively. For ESI and crystallographic data in CIF or other electronic format see DOI: 10.1039/d1mh01207j

This journal is © The Royal Society of Chemistry 2022

Published on 06 September 2021. Downloaded on 5/21/2025 1:41:29 AM.

photoinduced process. For instance, the photochromic process is competitive with photoluminescence in most cases, mainly related to the identical consumption of singlet or triplet state.

Herein, triphenylethylene with photochromic property is selected as the skeleton, which can demonstrate a photocyclization process under UV irradiation, resulting in an extended conjugation system with red-shifted absorption.[43–45] Moreover, some functional moieties are incorporated into the center double bond and/or peripheral phenyl moieties of triphenylethylene to adjust the molecular configurations and electronic properties. Notably, multi-photoresponsive properties with the combination of photochromism, photodeformation and RTP have been realized in these triphenylethylene derivatives, which are mainly related to the promoted photoinduced cyclization and ISC process by bromine substituents. Their electron-withdrawing properties can increase yields of photochemical reactions and extend absorption spectra. The heavy atom effect of bromine atoms benefits the ISC process, and molecular aggregates can be optimized by the additional C–H···Br interactions in the crystalline states, which are helpful to stabilize excited triplet states. As a result, all these triphenylethylene derivatives can exhibit photochromism, photodeformation and RTP simultaneously. Among these compounds, TPFBr2 exhibits the strongest absorption of 49% after UV irradiation, which is caused by the introduction of electron-withdrawing substituents including trifluoromethyl and bromine ones. Poly(ethylene terephthalate) (PET) film doped with 2.5 wt% TPMBr2 has the maximum photodeformation with bending angle of 130°, mainly due to the promoted interactions between PET matrix and TPMBr2 molecules by bromine substituents, while TPMBr exhibits persistent RTP emission with a lifetime of 297.0 ms and lasting for 150 min as detected by chemiluminescent imaging system.

Results and discussion

These compounds exhibited multi-responsive properties under UV irradiation, which are related to the photochemical reaction, and the radiative transition by photoexcitation (Fig. 1). All of them can be explained by the adjustable molecular conformations, intermolecular interactions and packing modes, which are dominated by the substituents to the central double bond and phenyl moieties. For photochromic and photodeformation properties, the photoinduced chemical reactions play the key role, which are mainly determined by the molecular conformations and electronic properties of photoactive phenyl moieties. RTP property is largely related to the molecular packing[46–50] and possible heavy atom effect, which affect the ISC process and the stability of excited triplet states at room temperature.

Photochromic property

These triphenylethylene derivatives are white powders or colorless crystals in the natural state (Fig. 2a). After UV irradiation (365 nm) for 5 s, the color can change to orange or purple rapidly, with peaks in the range of 480–520 nm appearing in the reflectance spectra (Fig. 2a and Fig. S1, ESI†). Either introduction of a bromine atom or the replacement of methyl group by trifluoromethyl resulted in the red shift of absorption as a result of their electron-withdrawing property. TPM turned to orange with a peak at 480 nm appearing in reflectance spectra under UV irradiation, while others exhibited purple color with peaks in the range of 512–520 nm in the reflectance spectra (Fig. 2b).

The photochromic process is rapid and tends to equilibration after UV irradiation of 5 s. However, this process cannot be expressed by the reflection spectra because of the large overlap of photoluminescence and reflection spectra under UV irradiation. Alternatively, the photochromic bleaching process can be shown by the reflectivity decay. As shown in Fig. 2b, reflectivities of TPF series after UV irradiation exhibit decreasing values with the incorporation of bromine atoms, from TPF (85%), to TPFBr (57%), then to TPFBr2 (51%). Since they exhibit a similar molar extinction coefficient (Fig. 2c), the trend indicates that the bromine substituent can promote the photoinduced cyclization process. This is mainly related to the molecular configurations in different conditions. The dihedral angles of photoactive phenyl moieties of TPF, TPFBr, and

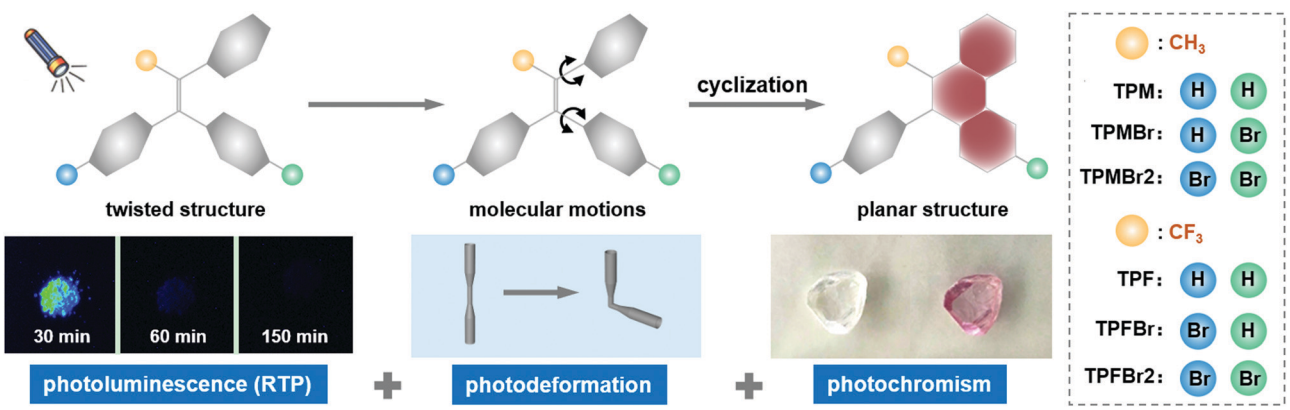

Fig. 1 Chemical structures and photoinduced cyclization process of triphenylethylene derivatives as well as schematic diagram of multi-photoresponsive properties.

Published on 06 September 2021. Downloaded on 5/21/2025 1:41:29 AM.

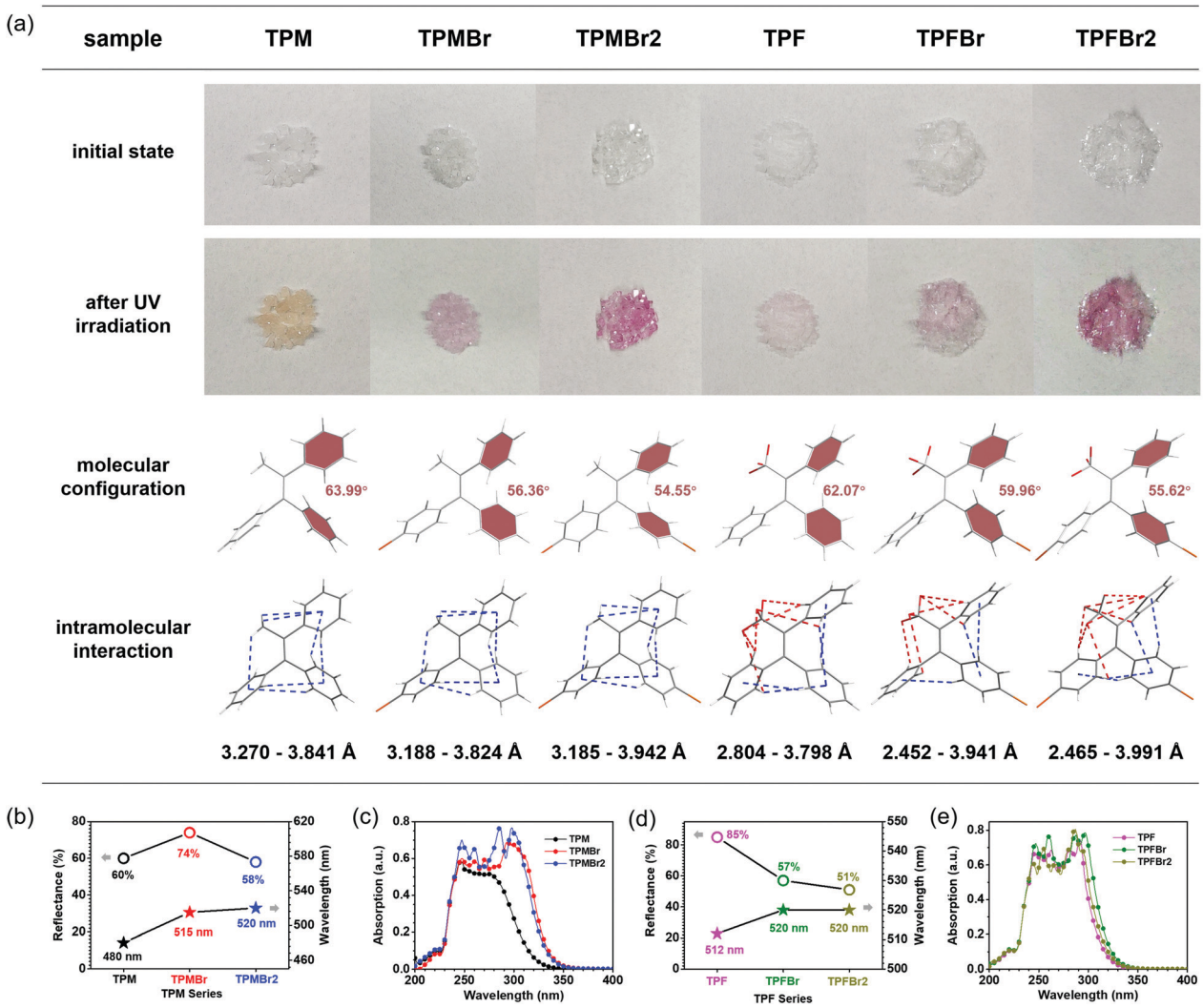

Fig. 2 (a) Photographs of triphenylethylene derivatives in initial state and after UV irradiation for 5 s, molecular conformations of triphenylethylene derivatives with dihedral angles between photoactive phenyl rings, intramolecular interactions of triphenylethylene derivatives and corresponding distances (C–H···π interactions are labeled by blue dotted lines and C–H···F interactions are labeled by red dotted lines). (b) Reflectance property of TPM series after UV irradiation for 5 s. (c) UV-visible absorption spectra of TPM series in DCM solution (1×10^{-5} mol L^{-1}). (d) Reflectance property of TPF series after UV irradiation for 5 s. (e) UV-visible absorption spectra of TPF series in DCM solution (1×10^{-5} mol L^{-1}).

TPFBr2 are 62.06°, 59.95° and 55.62°, respectively (Fig. 2d). The smaller dihedral angles of photoactive phenyl rings of the triphenylethylene skeleton in the initial state are close to those in the ring-closure state, beneficial to the cyclization process. As to the TPM series, the lowest reflectivity (58%) is achieved by TPMBr2 with two bromine substituents, which also proves the advantage of bromine atoms in the adjustment of molecular configurations. It demonstrated the smallest dihedral angles of photoactive phenyl rings (54.54°) in the TPM series. However, TPM exhibited lower reflectivity (60%) than TPMBr (74%), which is not only related to the involved dihedral angles, but also to the intramolecular interactions. Seven kinds of C–H···π interactions with average distance of 3.624 Å exist in TPM, while seven kinds of C–H···π interactions with average distance of 3.542 Å and 3.544 Å exist in TPMBr and TPMBr2, respectively. It is obvious that TPM possesses the weakest intramolecular interactions, which would decrease the hindrance for molecular motions under UV irradiation. Thus, the photoactive phenyl moieties can achieve the parallel mode from the twisted state rapidly, promoting to the photoinduced cyclization process. Also, a similar trend can be observed for the ground state (Fig. S2, ESI†).

Moreover, these triphenylethylene derivatives demonstrate great repeatability of photochromic capacities (Fig. S3, ESI†), favoring applications for data encryption or optical switching. The relatively weak photochromic capacity of TPF is attributed to the strong intramolecular interactions (C–H···F) and undesirable configurations with large dihedral angles between photoactive phenyl rings, which have an adverse impact on the photocyclization process. Also, the smaller change (less than 20%) of reflectance under different conditions resulted in the poor repeatability for low SNR (signal to noise ratio).

 This journal is © The Royal Society of Chemistry 2022

Published on 06 September 2021. Downloaded on 5/21/2025 1:41:29 AM.

Photodeformation property

The photodeformation property of these triphenylethylene derivatives was achieved with the assistance of PET as the matrix. The fabrication processes are shown in Fig. 3a, and PEDOT:PSS aqueous solution was spin-coated on a glass substrate before PET doped with 2.5% triphenylethylene derivatives was drop-cast. Then the doped PET film was separated from the glass substrate by being dipped in water and dried in a vacuum drying oven. All the doped PET films in the natural state exhibit nearly no photodeformation property under UV irradiation (365 nm), mainly due to the tiny change of triphenylethylene derivatives. Thus, with the aim of transferring the microscopic molecular motions to film deformation efficiently, the doped PET films are simply stretched in one direction to induce the crystallization process, according to our previous work.[24] All of the stretched films can shrink to the initial state after UV irradiation for 5 s (Fig. S5–S10, ESI†), and good repeatability can be realized by the stretching and photoinduced shrinking process alternately. The pure PET film cannot exhibit the photodeformation property in the stretched state (Fig. S4, ESI†), indicating the key role of these triphenylethylene derivatives in photoinduced cyclization activity. Even when the doped PET films were stretched to the break limit, they can roughly shrink to the initial length rapidly (Fig. S11 and S12, ESI†).

Also, the stretched films can be bent to a cylindrical state by UV stimulus to different degrees. The bending angles of TPM-PET, TPMBr-PET and TPMBr2-PET films are 85°, 101° and 130°, respectively, while those of TPF-PET, TPFBr-PET and TPFBr2-PET films are 30°, 70° and 75°, respectively. The obvious trend in both methyl- and trifluoromethyl-substituted triphenylethylene derivatives is that the doped films exhibited wider bending angles with the incorporation of bromine substituents. As mentioned above, the favorable conformations were achieved with smaller dihedral angles of photoactive phenyl moieties *via* the introduction of bromine substituents, contributing to the photocyclization process. Also, bromine substituents can induce possible hydrogen bonding between triphenylethylene derivatives and PET matrix, which can enhance their interactions, favoring the photodeformation process.

Thus, the photodeformation property should be derived from the molecular motions in the photoinduced cyclization reaction, and amplified by the polymer matrix with crystalline state and the interactions between triphenylethylene derivatives and PET. The bending angle as the key element of the photodeformation property is mainly determined by the degree of cyclization reaction, which exhibits the same trend as the photochromic property, and indicates the advantage of bromine substituents to peripheral phenyl moieties.

However, the TPF-PET series exhibited smaller bending angles than the TPM-PET series. This was mainly due to the additional C–H···F intramolecular interactions, which largely restricted the molecular motions. They may hinder the photocyclization process and decrease the amplitude of configuration variation, resulting in the weaker photodeformation property.

Room-temperature phosphorescence property

RTP property of organic materials is mainly determined by the ISC process and the stability of excited triplet states.[32–40] Until now, there have been no reports about the RTP effect of triphenylethylene derivatives, mainly due to the possible barrier in the ISC process. In our system, the six triphenylethylene derivatives exhibit an obvious RTP effect with different lifetimes and wavelengths. The introduction of bromine substituents increased the SOC between singlet and triplet excited states *via* the heavy atom effect, promoting the ISC process. Accordingly, the triphenylethylene derivatives with bromine

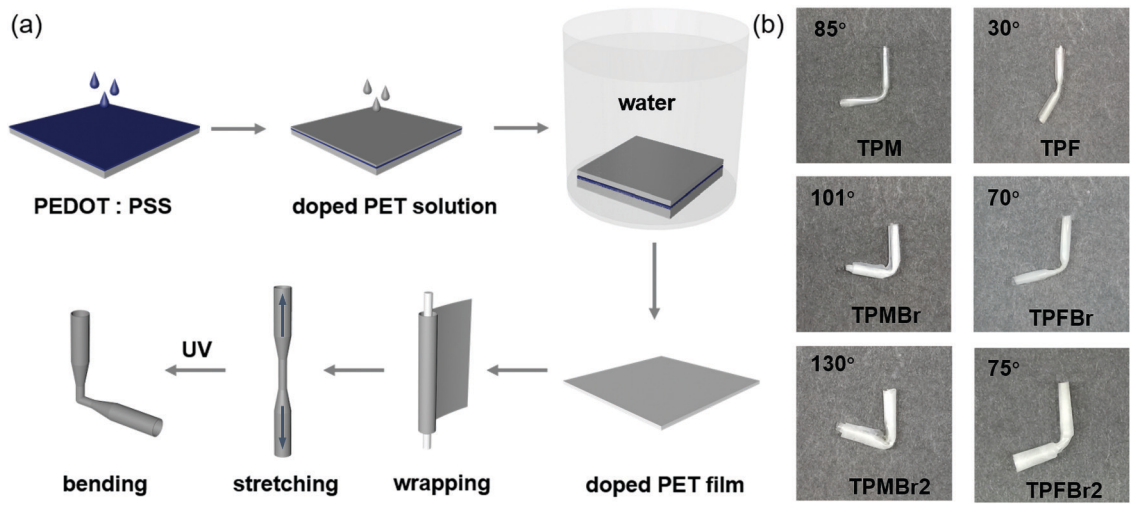

Fig. 3 (a) Schematic of doped PET film fabrication process (2.5 wt% triphenylethylene derivatives in PET) as well as photodeformation property. (b) Photographs of doped PET films (2 cm × 1 cm) with photoinduced bending process and corresponding bending angles (in the upper left corner of each picture).

Published on 06 September 2021. Downloaded on 5/21/2025 1:41:29 AM.

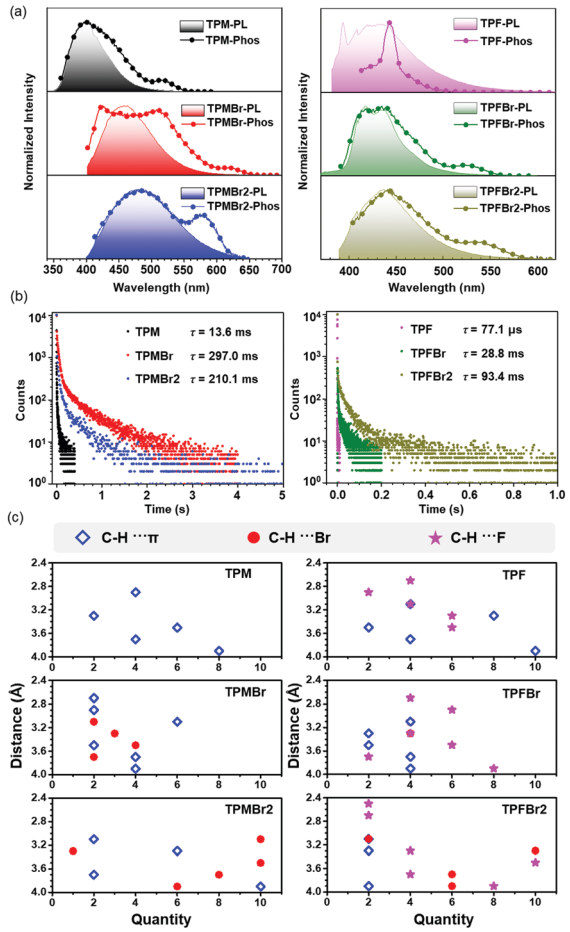

Fig. 4 (a) Photoluminescence and RTP spectra of triphenylethylene derivatives. (b) RTP decay of triphenylethylene derivatives. (c) The distance and quantity of intermolecular interactions of triphenylethylene derivatives from each molecule with adjacent ones in single crystals.

substituents exhibited much longer RTP lifetime in both TPM and TPF series, compared to those without bromine atoms. In the crystal state, the RTP lifetimes of TPM, TPMBr and TPMBr2 are 13.6 ms, 297.0 ms and 210.1 ms, respectively, while those of TPF, TPFBr and TPFBr2 are 77.1 μs, 28.8 ms and 93.4 ms, respectively (Fig. 4a and b). Also, the time that the afterglow lasted as detected by chemiluminescent imaging system exhibited a similar trend, and TPMBr exhibited the longest time up to 150 min (Fig. S13, ESI†). Moreover, the varied RTP effect is maintained after grinding, exhibiting a similar trend to that in single crystals (Fig. S14–S17 and Tables S1, S2, ESI†). Thus, the RTP effect of these triphenylethylene derivatives can be realized for different aggregated states, favoring their application in anti-counterfeiting and bioimaging fields.

The emission wavelengths of photoluminescence and RTP spectra were red-shifted with the incorporation of bromine, and the differences are larger in the TPM series (about 80 nm) than in the TPF series (about 40 nm). This was mainly related to the promoted intramolecular charge transfer by the electron-withdrawing property of bromine atoms. It can be further confirmed by the red shift of absorption spectra in dilute solution (1×10^{-5} mol L^{-1} in DCM). Also, the quantum yields of photoluminescence varied with the introduction of different numbers of bromine atoms, and mono-bromine-substituted triphenylethylene derivatives demonstrated the highest values both in TPM and TPF series in crystalline states. TPMBr exhibited photoluminescence quantum yield of 67.47%, higher than the 47.88% of TPM and 26.04% of TPMBr2.

The optimized photoluminescence and RTP property as a result of bromine atom introduction was not only related to the heavy atom effect, but also the additional C–H···Br interactions in the aggregated state. As shown in Fig. 4c, 11 and 35 kinds of C–H···Br interactions existed in TPMBr and TPMBr2 crystals among each molecule and adjacent ones, respectively, and their C–H···π interactions only exhibited a little change, compared to those of TPM without bromine atom. Thus, the whole molecular aggregates become rigid with the increased intermolecular interactions, which can suppress possible molecular motions, beneficial to the stability of the excited triplet state. A similar trend can be also observed in the TPF series (Fig. S18–S23, ESI†).

Furthermore, molecular packing exhibited subtle variations in these triphenylethylene derivatives due to the changeable molecular configurations and intermolecular interactions. In detail, the TPM series exhibited layer-by-layer stacking modes, roughly parallel to the center double bonds, while those of the TPF series are skewed to the center double bonds (Fig. 5 and Fig. S24, S25, ESI†). For the TPM series, the introduction of bromine atoms can result in compact molecular packing with decreased interlayer distances: in detail, 4.853 Å and 3.972 Å for TPMBr, and 4.383 Å and 4.362 Å for TPMBr2, with 5.130 Å and 4.639 Å for TPM as a reference. The smallest distance of 3.972 Å for TPMBr can benefit the electronic coupling of adjacent molecules in the aggregated state, contributing to the longest lifetime (297.0 ms) and lasting time (150 min) of RTP emission. In the TPF series, the effect of bromine atoms on molecular packing is less than that in the TPM series, mainly due to the existence of C–H···F interactions of 21, 24 and 29 kinds in TPF, TPFBr and TPFBr2, respectively. Their crystal structures exhibited the impact molecular packing with interlayer distances over 5.6 Å. Thus, the RTP lifetime in the TPF series exhibited an increasing trend with increasing number of bromine substituents, mainly determined by the heavy atom effect and intermolecular interactions.

It is worth mentioning that the *in situ* photoluminescence spectra of triphenylethylene derivatives exhibit nearly no change under UV irradiation for 60 s (Fig. S26, ESI†), regardless of the obvious color change at the same time. This might be related to the low photocyclization yields of triphenylethylene derivatives, which demonstrates the weak competition with the photoluminescence process in the excited states. Thus, multiple photoresponsive properties, including photochromism, photodeformation and RTP, can be realized in these triphenylethylene derivatives without obvious conflict, and mainly related to the different photoinduced processes under UV irradiation. Basically, the RTP effect is derived from the initial state of these compounds, which is promoted by the heavy

 This journal is © The Royal Society of Chemistry 2022

Published on 06 September 2021. Downloaded on 5/21/2025 1:41:29 AM.

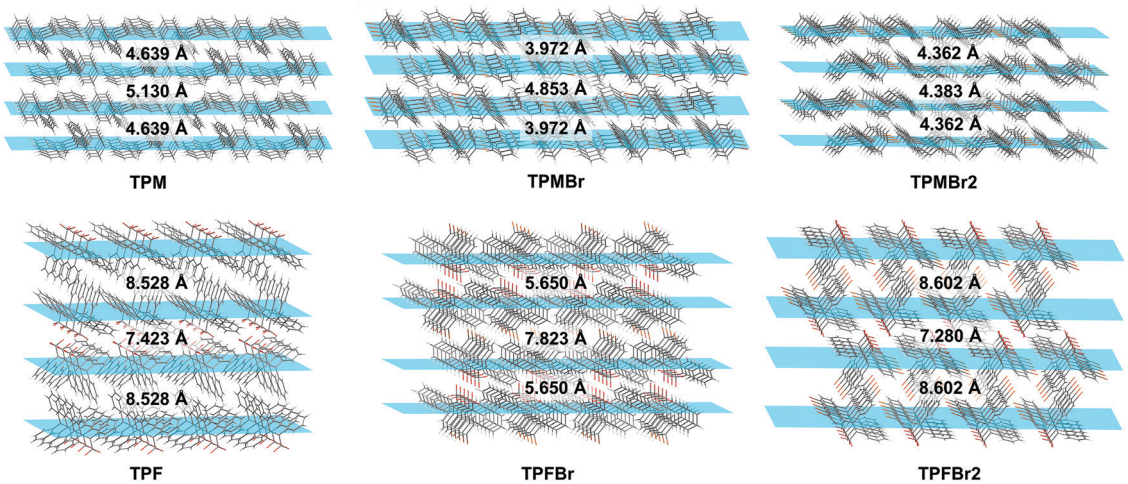

Fig. 5 Molecular packing of triphenylethylene derivatives in single crystals.

atom effect and strong intermolecular interactions. Photodeformation is induced by molecular motions during the photoinduced cyclization process, which is amplified by the well-organized aggregated structure of polymer matrix in the stretched state. Photochromism is related to the terminal state of photoinduced cyclization reaction, which exhibited enhanced intramolecular charge transfer by extended conjugation, resulting in the obvious color change in the solid state.

Conclusions

In summary, multiple photoresponsive properties, including photochromism, photodeformation and RTP, are realized in triphenylethylene derivatives for the first time. The dynamic photochromism and photodeformation processes are mainly due to the twisted triphenylethylene skeleton, and the photoinduced cyclization reaction promoted by bromine substituents. Accordingly, the heavy atom effect and the C–H···Br interactions promote ISC, and largely stabilize the excited triplet states, resulting in the persistent RTP. These photoresponsive properties heavily depend on molecular configurations and intermolecular interactions, which can be well adjusted by the position and number of bromine substituents. Thus, these results provide an efficient and simple strategy to achieve multiple photoresponsive properties by the rational design of molecular structures.

Experimental section

Instrumentation

Tetrahydrofuran was distilled from sodium potassium alloy under an atmosphere of argon. Chemical reagents and solvents were obtained commercially and used without further purification. ^{1}H and ^{13}C NMR spectra were recorded with a Bruker Avance III HD 400 MHz using tetramethylsilane (TMS; δ = 0 ppm) as internal standard. Elemental analyses were performed with a PerkinElmer microanalyzer. Mass spectra were measured using a ZAB 3F-HF mass spectrophotometer. Photoluminescence spectra, quantum yields and lifetimes were determined with an FLS980 spectrometer. The single-crystal X-ray diffraction data were collected with a Bruker Smart Apex CCD diffractometer. The time-dependent reflectance spectra and *in situ* photoluminescence were collected from an Ocean Optics QE65 Pro spectrometer. Afterglow photographs were taken with a Tanon 5200 Multi chemiluminescent imaging system. An LED irradiator (CCS, HLV-24GR-3W) was used as UV source in the photodeformation process.

The general synthesis route of triphenylethylene derivatives

Under an atmosphere of nitrogen, zinc powder (5.36 g, 82 mmol) and tetrahydrofuran (200 mL) were added in a 500 mL two-neck flask. After cooling to 0 °C, $TiCl_4$ (4.4 mL, 40 mmol) was added dropwise. The mixture was heated to 70 °C, and refluxed for 2 hours. Then, diphenyl ketone or 4-bromodiphenyl ketone or 4,4′-dibromodiphenyl ketone (10 mmol) and acetophenone or α,α,α-trifluoroacetophenone (10 mmol) were added. The resultant mixture was stirred at 70 °C overnight. After cooling to room temperature, water was added, and the mixture was extracted with dichloromethane several times. The combined organic layers were dried over anhydrous Na_2SO_4, and concentrated by rotary evaporation. The crude product was purified by recrystallization from hexane and/or by column chromatography on silica gel using petroleum ether as the eluent. All the target compounds were characterized by ^{1}H NMR, ^{13}C NMR, MS and EA (Fig. S27–S38, ESI†).

TPM. White solid (1.17 g, 43.2%). ^{1}H NMR (400 MHz, CD_2Cl_2) δ (ppm): 7.42–7.38 (m, 2H, ArH), 7.33–7.28 (m, 3H, ArH), 7.19–7.12 (m, 5H, ArH), 7.10–7.04 (m, 3H, ArH), 6.96–6.94 (m, 2H, ArH), 2.15 (s, 3H, CH_3). ^{13}C NMR (100 MHz, CD_2Cl_2) δ (ppm): 144.11, 143.55, 143.26, 139.26, 135.83, 130.67, 129.77, 129.22, 128.12, 127.75, 127.38, 126.54, 126.10, 125.76, 23.07. MS (EI, *m*/*z*): calcd for $C_{21}H_{18}$, 270.38; found, 270.10. Anal. calcd for $C_{21}H_{18}$: C, 93.29; H, 6.71. Found: C, 93.02; H, 6.75.

Published on 06 September 2021. Downloaded on 5/21/2025 1:41:29 AM.

TPMBr. White solid (312 mg, 4.5%). ^{1}H NMR (400 MHz, CD_2Cl_2) δ (ppm): 7.55–7.51 (m, 2H, ArH), 7.20–7.14 (m, 7H, ArH), 7.09–7.05 (m, 3H, ArH), 7.10–7.04 (m, 3H, ArH), 6.95–6.92 (m, 2H, ArH), 2.15 (s, 3H, CH_3). ^{13}C NMR (100 MHz, CD_2Cl_2) δ (ppm): 143.81, 142.74, 142.52, 138.08, 136.55, 131.67, 131.25, 130.70, 129.15, 127.80, 127.48, 126.27, 125.98, 120.41, 23.09. MS (EI, *m*/*z*): calcd for $C_{21}H_{17}Br$, 349.27; found, 350.05. Anal. Calcd for $C_{21}H_{17}Br$: C, 72.22; H, 4.91. Found: C, 72.40; H, 4.85.

TPMBr2. White solid (1.11 g, 26.8%). ^{1}H NMR (400 MHz, $CDCl_3$) δ (ppm): 7.49–7.47 (m, 2H, ArH), 7.20–7.08 (m, 9H, ArH), 6.73–6.71 (m, 2H, ArH), 2.11 (s, 3H, CH_3). ^{13}C NMR (100 MHz, CD_2Cl_2) δ (ppm): 143.29, 141.87, 141.50, 137.24, 136.97, 132.49, 131.77, 131.45, 130.73, 129.11, 128.16, 126.68, 120.88, 120.14, 23.47. MS (EI, *m*/*z*): calcd for $C_{21}H_{16}Br_2$, 428.17; found, 427.90. Anal. calcd for $C_{21}H_{16}Br_2$: C, 58.91; H, 3.77. Found: C, 59.05; H, 3.66.

TPF. White solid (0.86 g, 26.6%). ^{1}H NMR (400 MHz, $CDCl_3$) δ (ppm): 7.39–7.30 (m, 5H, ArH), 7.25–7.19 (m, 5H, ArH), 7.04–7.02 (m, 3H, ArH), 6.93–6.91 (m, 2H, ArH). ^{13}C NMR (100 MHz, CD_2Cl_2) δ (ppm): 150.36, 140.94, 140.49, 135.00, 131.42, 129.65, 129.28, 128.50, 128.01, 127.93, 127.86, 127.70, 127.36, 124.99, 122.25. MS (EI, *m*/*z*): calcd for $C_{21}H_{15}F_3$, 324.35; found, 324.05. Anal. calcd for $C_{21}H_{15}F_3$: C, 77.77; H, 4.66. Found: C, 77.50; H, 4.60.

TPFBr. White solid (0.21 g, 5.3%). ^{1}H NMR (400 MHz, CD_2Cl_2) δ (ppm): 7.47–7.41 (m, 3H, ArH), 7.36–7.34 (m, 2H, ArH), 7.31 (s, 5H, ArH), 7.26–7.23 (m, 2H, ArH), 6.89–6.86 (m, 2H, ArH). ^{13}C NMR (100 MHz, CD_2Cl_2) δ (ppm): 149.35, 139.95, 134.53, 131.25, 130.90, 129.88, 129.60, 128.37, 128.35, 128.13, 128.09, 124.92, 122.18, 121.55, 119.45. MS (EI, *m*/*z*): calcd for $C_{21}H_{14}F_3Br$, 403.24; found, 403.95. Anal. calcd for $C_{21}H_{14}F_3Br$: C, 62.55; H, 3.50. Found: C, 62.44; H, 3.33.

TPFBr2. White solid (1.21 g, 25.2%). ^{1}H NMR (400 MHz, CD_2Cl_2) δ (ppm): 7.55–7.52 (m, 2H, ArH), 7.27–7.17 (m, 9H, ArH), 6.82–6.78 (m, 2H, ArH). ^{13}C NMR (100 MHz, CD_2Cl_2) δ (ppm): 148.05, 139.37, 138.88, 134.25, 131.36, 131.30, 131.16, 131.01, 130.21, 128.28, 128.18, 124.79, 122.33, 122.05, 121.82. MS (EI, *m*/*z*): calcd for $C_{21}H_{13}F_3Br_2$, 482.14; found, 481.85. Anal. calcd for $C_{21}H_{13}F_3Br_2$: C, 52.32; H, 2.72. Found: C, 52.43; H, 2.56.

Author contributions

Q. L. and Z. L. conceived the project. Y. F. synthesized all of the materials and performed all the measurements. M. H. performed part of single-crystal measurements. A. H. helped to measure the photodeformation capacities. Q. L. performed part of single-crystal measurements and helped to take afterglow photographs. J. T., X. L. and B. H. performed a part of the synthetic experiments. Q. L. and Z. L. discussed and revised the manuscript. All of the authors approved the manuscript.

Conflicts of interest

There are no conflicts to declare.

Acknowledgements

We are grateful to the National Natural Science Foundation of China (no. 21734007, 51973162, 21875174), Excellent Youth Foundation of Hubei Scientific Committee (2020CFA084), the Fundamental Research Funds for the Central Universities (2042020kf0200) and Wuhan City (2019010701011412) for financial support.

Notes and references

1 A. Fihey, A. Perrier, W. R. Browne and D. Jacquemin, *Chem. Soc. Rev.*, 2015, **44**, 3719–3759.
2 P. Wei, J. X. Zhang, Z. Zhao, Y. Chen, X. He, M. Chen, J. Gong, H. H. Sung, I. D. Williams, J. W. Y. Lam and B. Z. Tang, *J. Am. Chem. Soc.*, 2018, **140**, 1966–1975.
3 K. Zheng, S. Han, X. Zeng, Y. Wu, S. Song, H. Zhang and X. Liu, *Adv. Mater.*, 2018, **30**, 1801726.
4 R. Klajn, *Chem. Soc. Rev.*, 2014, **43**, 148–184.
5 S. Tang, F. Song, M. Lu, K. Han and X. Peng, *Sci. China: Chem.*, 2019, **62**, 451–459.
6 A. B. Abood and M. A. Abdullah, *Chin. J. Polym. Sci.*, 2008, **26**, 433–441.
7 G. Pan, J. Wei, A. Zhu, Y. Ming, M. Fan and S. Yao, *Sci. China, Ser. B: Chem.*, 2001, **44**, 276–282.
8 Y. Ming, Z. Huang, M. Fan and B. Xu, *Sci. China, Ser. B: Chem.*, 1997, **40**, 373–379.
9 S. Wang, F. Wang, C. Li, T. Li, D. Cao and X. Ma, *Sci. China: Chem.*, 2018, **61**, 1301–1306.
10 T. Huang, H. Liu, Y. Bang, Y. Wang, Y. Liang, X. Wang, Y. Zhang, S. Xie and Z. Zheng, *Sci. China: Chem.*, 2020, **63**, 1659–1665.
11 O. Tosic, K. Altenhoner and J. Mattay, *Photochem. Photobiol. Sci.*, 2010, **9**, 128–130.
12 M. Herder, B. M. Schmidt, L. Grubert, M. Patzel, J. Schwarz and S. Hecht, *J. Am. Chem. Soc.*, 2015, **137**, 2738–2747.
13 N. M.-W. Wu, M. Ng, W. H. Lam, H.-L. Wong and V. W.-W. Yam, *J. Am. Chem. Soc.*, 2017, **139**, 15142–15150.
14 C. P. Harvey and J. D. Tovar, *Polym. Chem.*, 2011, **2**, 2699–2706.
15 S. Zhou, S. Guo, W. Liu, Q. Yang, H. Sun, R. Ding, Z. Qian and H. Feng, *J. Mater. Chem. C*, 2020, **8**, 13197–13204.
16 S. Fredrich, R. Göstl, M. Herder, L. Grubert and S. Hecht, *Angew. Chem., Int. Ed.*, 2016, **55**, 1208–1212.
17 J. Li, X. Zhou and Z. Liu, *Adv. Opt. Mater.*, 2020, **8**, 2000886.
18 H. K. Bisoyi and Q. Li, *Chem. Rev.*, 2016, **116**, 15089–15166.
19 Y. Naka, J. Mamiya, A. Shishido and T. Ikeda, *Mol. Cryst. Liq. Cryst.*, 2011, **547**, 1832–1841.
20 M. Kim, J. H. Yun and M. Cho, *Sci. Rep.*, 2017, **7**, 967.
21 B. Xu, C. Y. Zhu, L. Qin, J. Wei and Y. L. Yu, *Small*, 2019, **15**, 1901847.
22 P. P. Zhang, Z. X. Lan, J. Wei and Y. L. Yu, *ACS Macro Lett.*, 2021, **10**, 469–475.
23 Y. Liu, S. Sun and S. Wu, *Chin. J. Chem.*, 2020, **38**, 1019–1022.
24 A. Huang, J. Hu, M. Han, K. Wang, J. L. Xia, J. Song, X. Fu, K. Chang, X. Deng, S. Liu, Q. Li and Z. Li, *Adv. Mater.*, 2021, **33**, 2005249.

 This journal is © The Royal Society of Chemistry 2022

Published on 06 September 2021. Downloaded on 5/21/2025 1:41:29 AM.

25 T. Ube and T. Ikeda, *Adv. Opt. Mater.*, 2019, **7**, 1900380.
26 B. Zuo, M. Wang, B. P. Lin and H. Yang, *Nat. Commun.*, 2019, **10**, 4539.
27 Z. Z. Wang and H. Q. Zhang, *Chin. J. Polym. Sci.*, 2020, **38**, 37–44.
28 S. Q. Han, Y. Y. Chen and B. Xu, *Chin. J. Polym. Sci.*, 2020, **38**, 806–813.
29 H. T. Yu, J. W. Tang, Y. Y. Feng and W. Feng, *Chin. J. Polym. Sci.*, 2019, **37**, 1183–1199.
30 S. Huang, Y. Huang and Q. Li, *Small Struct.*, 2021, 2100038.
31 Y. Huang, H. K. Bisoyi, H. Huang, M. Huang, M. Wang, X. M. Chen, Z. liu, H. Yang and Q. Li, *Angew. Chem., Int. Ed.*, 2021, **60**, 11247–11251.
32 Y. Tani, M. Komura and T. Ogawa, *Chem. Commun.*, 2020, **56**, 6810–6813.
33 Q. Liao, Q. Gao, J. Wang, Y. Gong, Q. Peng, Y. Tian, Y. Fan, H. Guo, D. Ding, Q. Li and Z. Li, *Angew. Chem., Int. Ed.*, 2020, **59**, 9946–9951.
34 J. Yang, M. Fang and Z. Li, *InfoMat*, 2020, **2**, 791–806.
35 Q. Liao, Q. Li and Z. Li, *ChemPhotoChem*, 2021, **5**, 694–701.
36 Z. Chai, C. Wang, J. Wang, F. Liu, Y. Xie, Y. Z. Zhang, J. R. Li, Q. Li and Z. Li, *Chem. Sci.*, 2017, **8**, 8336–8344.
37 Y. Wang, J. Yang, Y. Tian, M. Fang, Q. Liao, L. Wang, W. Hu, B. Z. Tang and Z. Li, *Chem. Sci.*, 2020, **11**, 833–838.
38 W. Che, Y. Gong, L. Tu, M. Han, X. Li, Y. Xie and Z. Li, *Phys. Chem. Chem. Phys.*, 2020, **22**, 21445–21452.
39 J. Wang, Z. Chai, J. Wang, C. Wang, M. Han, Q. Liao, A. Huang, P. Lin, C. Li, Q. Li and Z. Li, *Angew. Chem., Int. Ed.*, 2019, **58**, 17297–17302.
40 Q. Dang, L. Hu, J. Wang, Q. Zhang, M. Han, S. Luo, Y. Gong, C. Wang, Q. Li and Z. Li, *Chem. – Eur. J.*, 2019, **25**, 7031–7037.
41 M. Fang, J. Yang, X. Xiang, Y. Xie, Y. Dong, Q. Peng, Q. Li and Z. Li, *Mater. Chem. Front.*, 2018, **2**, 2124–2129.
42 J. Yang, X. Zhen, B. Wang, X. Gao, Z. Ren, J. Wang, Y. Xie, J. Li, Q. Peng, K. Pu and Z. Li, *Nat. Commun.*, 2018, **9**, 840.
43 D. P. Ou, T. Yu, Z. Y. Yang, T. G. Luan, Z. Mao, Y. Zhang, S. W. Liu, J. R. Xu, Z. G. Chi and M. R. Bryce, *Chem. Sci.*, 2016, **7**, 5302–5306.
44 L. Wang, T. Yu, Z. Xie, X. Chen, Z. Yang, Y. Zhang, M. P. Aldred and Z. Chi, *J. Mater. Chem. C*, 2018, **6**, 8832–8838.
45 T. Yu, D. Ou, L. Wang, S. Zheng, Z. Yang, Y. Zhang, Z. Chi, S. Liu, J. Xu and M. P. Aldred, *Mater. Chem. Front.*, 2017, **1**, 1900–1904.
46 Q. Li and Z. Li, *Acc. Chem. Res.*, 2020, **53**, 962–973.
47 F. Liu, Q. Liao, J. Wang, Y. Gong, Q. Dang, W. Ling, M. Han, Q. Li and Z. Li, *Sci. China: Chem.*, 2020, **63**, 1435–1442.
48 J. Yang, Z. Chi, W. Zhu, B. Z. Tang and Z. Li, *Sci. China: Chem.*, 2019, **62**, 1090–1098.
49 M. Fang, J. Yang and Z. Li, *Chin. J. Polym. Sci.*, 2019, **37**, 383–393.
50 Q. Li and Z. Li, *Sci. China Mater.*, 2020, **63**, 177–184.